Phenolate-bridged A_2B-type subporphyrin dimer

Hirokawa, Shoma
Department of Chemistry, Graduate School of Science, Tohoku University

Mori, Shigeki
Advanced Research Support Center (ADRES), Ehime University

Kobayashi, Nagao
Department of Chemistry, Graduate School of Science, Tohoku University

Shimizu, Soji
Department of Chemistry and Biochemistry, Graduate School of Engineering, Kyushu University

出版情報：Journal of Porphyrins and Phthalocyanines. 25 (10n12), pp.975-980, 2021-07-26. World Scientific Publishing
バージョン：
権利関係：

Phenolate-bridged A_2B-type subporphyrin dimer

Shoma Hirokawa[a], Shigeki Mori[b], Nagao Kobayashi[*a,c◊] and Soji Shimizu[*d◊]

[a] *Department of Chemistry, Graduate School of Science, Tohoku University, Sendai 980-8578, Japan*

[b] *Advanced Research Support Center (ADRES), Ehime University, Matsuyama 790-8577, Japan*

[c] *Faculty of Textile Science and Technology, Shinshu University, Ueda 386-8567, Japan*

[d] *Department of Chemistry and Biochemistry, Graduate School of Engineering and Center for Molecular Systems (CMS), Kyushu University, Fukuoka 819-0395, Japan*

Dedicated to the 70th birthday of Prof. Lechosław Latos-Grażyński and the 65th birthday of Prof. Hiroyuki Furuta

Received date (to be automatically inserted after your manuscript is submitted)
Accepted date (to be automatically inserted after your manuscript is accepted)

ABSTRACT: An ether cleavage reaction of A_2B-type subporphyrin bearing an *ortho*-anisyl substituent afforded a phenolate-bridged dimer. A head-to-tail structure of the dimer was unambiguously elucidated by single crystal X-ray diffraction analysis. UV/vis absorption and magnetic circular dichroism spectra indicated a minor interaction between the subporphyrin chromophores. Density functional theory calculations provided a detailed insight into the electronic structures of the subporphyrin dimer.

KEYWORDS: subporphyrin, head-to-tail dimer, UV/vis and MCD spectroscopies

◊ SPP full member in good standing

*Correspondence to: Nagao Kobayashi, email: nagaok@shinshu-u.ac.jp and Soji Shimizu, email: ssoji@cstf.kyushu-u.ac.jp, fax: +81-92-802-2866

For celebration issue on the occasion of the 70th birthday of Prof. Lechosław Latos-Grażyński and the 65th birthday of Prof. Hiroyuki Furuta

INTRODUCTION

Subporphyrin is a contracted porphyrin analog comprising three pyrrole rings bridged to each other by a methine carbon atom [1]. In contrast to its structural analogs, subpyriporphyrin [2] and triphyrins [3–6], subporphyrin has been exclusively obtained as its boron complex because the trigonal pyramidal coordination of boron plays a crucial role in forming the tripyrrolic core structure of subporphyrin: tribenzosubporphyrin is synthesized from (3-oxo-2,3-dihydro-1*H*-isoindol-1-yl)acetic acid or phthalimide and arylacetic acid using boric acid as a template [7–9], whereas *meso*-aryl-substituted subporphyrin is synthesized from tripyrrolylborane as a key precursor [10–12]. In addition to the indispensable role of the central boron in the synthesis, its axial reactivity is also a unique feature of subporphyrin. For example, in an axial ligand exchange reaction of *B*-alkoxy and *B*-hydroxy subporphyrins, bowl-to-bowl inversion occurs via a planar borenium cation intermediate formed in a S_N1-type heterolysis of the B–O bond [13]. The axial reactivity can also be used for creating molecular assemblies such as a face-to-face homo-dimer, a face-to-face hetero-triad with phthalocyanine [14] and head-to-tail homo-dimer and homo-trimer [15, 16] (Fig. 1). Recently, in the synthesis of the peripherally-fused chiral subporphyrin from A_2B-type subporphyrin bearing an *ortho*-anisyl substituent [17], we accidentally obtained a phenolate-bridged head-to-tail subporphyrin dimer, in which the *ortho*-hydroxyphenyl group at the *meso*-position formed a B–O bond with the adjacent molecule. Despite the slipped stacking structure in close proximity, this dimer exhibited similar UV/vis absorption and magnetic circular dichroism (MCD) spectra to those of the corresponding monomer. Here, we report the synthesis and optical properties of the phenolate-bridged dimer and discuss its electronic structure based on the density functional theory (DFT) calculations.

(Fig. 1)

Fig. 1. (a) Face-to-face homo-dimer (left) and hetero-triad with phthalocyanine (right) and (b) head-to-tail homo-dimer (left) and homo-trimer (right).

EXPERIMENTAL

General procedure

High-resolution mass spectrometry (HR-MS) was performed on a Bruker Daltonics solariX 9.4T spectrometer (FT-ICR (Fourier transform ion cyclotron resonance) mode). ^{1}H NMR spectra were recorded on a Bruker AVANCE 500 (operating at 500.133 MHz) spectrometer using the residual solvent as an internal reference for ^{1}H (δ = 7.26 ppm for $CDCl_3$). Electronic absorption spectra were recorded on a JASCO V-570 spectrophotometer. Fluorescence spectra and absolute fluorescence quantum yields were measured using a Hamamatsu Photonics A10104-01 calibrated integrating sphere system. MCD spectra were recorded on a JASCO J-725 spectrodichrometer by applying parallel and antiparallel magnetic fields to the light propagation with an electromagnet, which produces magnetic fields of up to 1.03 T (1T = 1 tesla). The magnitudes were expressed in terms of molar ellipticity per tesla ($[\theta]_M$/deg dm^3 mol^{-1} cm^{-1} T^{-1}). Preparative separations were performed by silica gel column chromatography (Silica gel 60, Merck), alumina gel column chromatography (Wako), gel permeation chromatography (GPC) (Bio-Beads S-X1) and recycling preparative GPC-HPLC (JAI LC-9210 NEXT with preparative JAIGEL-2.5H and 3H columns). All reagents and solvents were of commercial reagent grade and were used without further purification except where noted.

Crystallographic data collection and structure refinement

Data collection was conducted at 100 K on a Rigaku R-AXIS RAPID diffractometer with CuKα radiation (λ = 1.54187 Å). The structure was solved by direct methods (SIR2011 [18]) and refined using a full-matrix least squares technique (SHELXL [19]). CCDC-2081138 contains the supplementary crystallographic data.

Theoretical calculation details

The Gaussian 16 software package [20] was used to perform DFT and TD-DFT calculations using the CAM-B3LYP functional [21] with 6-31G(d) basis set [22]. For the model structure of **4**, an axially chloro-substituted structure was used for simplicity. The hole-electron analysis was conducted by Multiwfn [23, 24].

Synthesis of a phenolate-bridged subporphyrin dimer (2)

Methoxo(5-*ortho*-anisyl-10,15-diphenylsubporphyrinato)boron(III) **1** was synthesized according to the literature procedure [13]. To a dichloromethane solution of **1** (50 mg, 0.094 mmol) was added a 1 M dichloromethane solution of boron tribromide (1.0 mL, 10.6 eq). The mixture was stirred for three hours at room temperature, then washed with brine, and the organic layer was extracted. After removal of solvent, the obtained mixture was roughly purified by gel permeation chromatography (Bio-Beads S-X1) using THF as an eluent. The fraction containing the dimer (**2**) was further purified by recycling GPC-HPLC (JAI LC-9210 NEXT with preparative JAIGEL-2.5H and 3H columns) using chloroform as an eluent. **2** was obtained in 8.8% yield (4.0 mg, 8.3 μmol) after recrystallization from dichloromethane and hexane. HRMS (MALDI-FT-ICR): *m/z* 970.33930 (calcd for $C_{66}H_{40}B_2O_2$ [M$^+$] 970.33934). ^{1}H NMR (500 MHz, $CDCl_3$, 298 K): δ_H, ppm 8.21 (s, 4H), 7.99 (d, J = 7.5 Hz, 8H), 7.74 (d, J = 4.5 Hz, 4H), 7.69 (dd, $J_1 = J_2$ = 7.5 Hz, 8H), 7.60 (t, J = 7.5 Hz, 4H), 7.33 (d, J = 4.5 Hz, 4H), 6.98 (ddd, $J_1 = J_2$ = 7.8 Hz, J_3 = 2.0 Hz, 2H), 6.74 (ddd, $J_1 = J_2$ = 7.8 Hz, J_3 = 1.0 Hz, 2H), 6.63 (dd, J_1 = 7.8 Hz, J_2 = 2.0 Hz, 2H), 5.36 (dd, J_1 = 7.8 Hz, J_2 = 1.0 Hz, 2H). UV/vis (CH_2Cl_2): λ, nm (ε, M^{-1} cm^{-1}) 460 (20000), 370 (180000).

RESULTS AND DISCUSSION

In the synthesis of the peripherally-fused chiral subporphyrin, an ether cleavage reaction of 5-*ortho*-anisyl-10,15-diphenyl-substituted subporphyrin **1** [13] was attempted. Together with the target *ortho*-hydroxyphenyl-substituted subporphyrin **3**, a phenolate-bridged dimer (**2**) was also formed due to the simultaneous dimerization of **3** (Scheme 1). Because of the difficulty in purification of **3** at this stage, a mixture of **2** and **3** was used for the synthesis of the peripherally-fused chiral subporphyrin in the previous study [17]. Therefore, the axial ligand of **3** was not determined. In contrast, **2** could be isolated by gel permeation column chromatography and obtained in 8.8% yield, and the structure was characterized.

(Scheme 1)

Scheme 1. Synthesis of the phenolate-bridged dimer (**2**) and *ortho*-hydroxyphenyl-substituted subporphyrin **3**. The axial ligand of **3** denoted by X was not determined.

The dimeric structure of **2** was confirmed by the high-resolution mass spectrometry (Fig. S1), and the head-to-tail phenolate-bridged structure was unambiguously elucidated by X-ray diffraction analysis (Fig. 2) [25]. In the crystal structure, the convex surfaces of the two subporphyrins are slipped and stacked with a distance of ca. 3.6 Å between the linking *meso*-carbon atom and the boron atom. The B–O–*ortho*-C bonds point in the same direction so that the mean planes of the two subporphyrins are slightly tilted. In the ^{1}H NMR spectrum of **3** (Fig. S2), the proton signals of the

linking *ortho*-hydroxyphenyl substituents are shifted upfield (6.98–5.36 ppm) due to the diatropic ring current effect of the adjacent aromatic subporphyrin ring. Except for one pyrrolic β-proton signal at 7.33 ppm, which can be assigned to the β-protons adjacent to the linking *meso*-positions, two other types of β-protons resonate at almost similar chemical shifts to those of the monomeric subporphyrins (ca. δ = 7.7–8.3 ppm), implying minor ring current effects around the outer periphery.

(Fig. 2)

Fig. 2. X-ray single crystal structure of **2**, (a) side view and (b) top view. The thermal ellipsoids are scaled to the 50% probability level. Hydrogen atoms and *meso*-phenyl-substituents are omitted for clarity.

In the UV/vis absorption spectrum in dichloromethane, **2** exhibits the Soret band at 368 nm and the Q band and its shoulder at 460 and 485 nm, respectively (Fig. 3). Corresponding to the Q band absorption (450–520 nm), two couples of Faraday *B* terms with negative-to-positive (500 and 484 nm) and positive-to-negative (462 and 445 nm) envelopes are observed in the magnetic circular dichroism (MCD) spectrum [26, 27]. In contrast to the complex MCD spectrum in the Q band region, the Soret band region is characterized by a large negative MCD envelop at 366 nm. Despite the slight blue shift of the Soret band by 5 nm, both the UV/vis absorption and MCD spectra of **2** resemble those of *meso*-phenyl-substituted subporphyrin [11]. In comparison with **1**, there is no significant change in the Q band region, whereas the Soret band of **2** is slightly broadened (Fig. S3). These results indicate a minor inter-chromophore interaction between subporphyrin chromophores in the dimeric structure of **2**. The fluorescence spectrum of **2** with a similar fluorescence quantum yield (0.12) to those of *meso*-aryl-substituted subporphyrins also supports a small perturbation between the monomer units (Fig. 3).

The anomalous MCD spectrum of **2** is typical of *meso*-aryl-substituted subporphyrins, which exhibit various MCD spectral profiles depending on the types of *meso*-aryl substituents [11]. According to Michl's perimeter model for the prediction of MCD sign sequences, aromatic 4N+2 π systems with non-degenerate HOMO and HOMO–1 and degenerate LUMO such as porphyrin normally exhibit negative-to-positive sign sequences in ascending energy [28–30]. By calculating the magnetic moments of the excited states, Ceulemans et al. revealed that quenching of the magnetic moments of the excited electrons by the *meso*-aryl substituents causes the observed MCD sign anomaly of subporphyrins [31]. The complex MCD sign sequence of **2** can also be explained by considering that **2** consists of two *meso*-phenyl-substituted subporphyrin with minor inter-chromophore interactions.

(Fig. 3)

Fig. 3. UV/vis absorption (bottom, solid line), fluorescence (bottom, dashed line), and MCD (top) spectra of **2** in CH_2Cl_2.

To provide a detailed insight into the electronic transitions of **2**, theoretical calculations were performed using time-dependent density functional theory (TD-DFT) at the CAM-B3LYP/6-31G(d) level, and the calculation results were compared with those of *meso*-phenyl-substituted subporphyrin with an axial chlorine ligand (**4**) as a reference compound (Fig. 4 and Table S1–S4). Similarly to porphyrin, the absorption spectrum of subporphyrin can be described based on Gouterman's four orbital model [32, 33]. This model explains that the intense Soret bands and weak Q bands result from the configurational interactions of transitions from the HOMO and HOMO–1 to the nearly degenerate LUMO. The TD-DFT calculation on **4** nicely reproduces the absorption properties of subporphyrin described by Gouterman's four orbital model: the four frontier MOs of **4** contribute to the two bands at 431 nm with small oscillator strengths (*f*) of 0.047 and 0.037 and two intense bands at 325 nm (f = 0.99) and 324 nm (f = 0.99), which can be ascribed to the Q and Soret bands, respectively (Table S1). Three nodal planes of the HOMO and HOMO–1 and four nodal planes of the LUMO and LUMO+1 also reflect the 14π-electron aromatic conjugation of **4**. The MO distribution

patterns of **2** clearly demonstrate that the eight frontier MOs of **2** from the HOMO–3 to the LUMO+3 are linear combination products of the four frontier MOs of **4** (Fig. 4). Due to the small MO interaction of the HOMO of the monomer unit, the HOMO and HOMO–1 of **2** are nearly degenerate, whereas the rather significant MO interaction of the HOMO–1 of the monomer unit results in the HOMO–2 and HOMO–3 lying with the energy difference of 0.15 eV. These frontier MOs contribute to the four weak bands (427, 428 and 431 nm) in the Q band region and several bands (336–292 nm) in the Soret band region (Table S2), which reproduces the slightly broadened Soret band and negligible changes in the Q band compared with **1**. These calculation results indicate minor inter-chromophore interactions in the Q band region and small ones in the Soret band region. The hole-electron analysis on the first four transitions corresponding to the Q bands reveals similar hole and electron distribution patterns to those of the Q bands of **4** (Figs. S4–S5), supporting the minor inter-chromophore interactions in the Q band region [23, 24].

(Fig. 4)

Fig. 4. Partial frontier MO diagram of **2** (left) and **4** (right) at the CAM-B3LYP/6-31G(d) level. Top (top) and side (bottom) views of MOs are shown for **2**. In the top views of **2**, subporphyrin cores are highlighted in light blue and yellow. Nodal planes of frontier MOs of **4** are shown by green dotted lines.

CONCLUSIONS

In summary, a phenolate-bridged subporphyrin dimer was obtained by an ether cleavage reaction of A_2B-type subporphyrin bearing an *ortho*-anisyl substituent. Despite the spatial proximity between the two subporphyrin chromophores, the dimer exhibited similar UV/vis absorption, MCD and fluorescence spectra, indicating the minor inter-chromophore interactions. The theoretical calculations strongly supported these observed results, and the hole-electron analysis on transitions was demonstrated to be a powerful tool for estimating the inter-chromophore interactions of assembled molecular systems. Considering that the present head-to-tail dimer structure was formed because of the presence of the hydroxy group at the *ortho*-position, *meta*- and *para*-hydroxyphenyl-substituted subporphyrin can form other types of oligomer assemblies. Research along this direction is of great interest and is currently being investigated in our laboratory.

Acknowledgement

This work was supported by Grants-in-Aid for Scientific Research (B), Scientific Research (C) and Scientific Research on Innovative Areas, "π-system Figuration: Control of Electron and Structural Dynamism for Innovative Functions (no. 2601)" (JSPS KAKENHI Grant numbers JP19H02703, JP18K05076, JP15H01001 and JP17H05160).

Supporting Information

Crystallographic data have been deposited at the Cambridge Crystallographic Data Centre (CCDC) under number CCDC-2081138. Copies can be obtained on request, free of charge, *via* http://www.ccdc.cam.ac.uk/ data_request/cif or from the Cambridge Crystallographic Data Centre, 12 Union Road, Cambridge CB2 1EZ, UK (fax: +44 1223-336-033 or email: deposit@ccdc.cam. ac.uk).

REFERENCES

1. Shimizu S. *Chem. Rev*. 2017; **117**: 2730-2784.
2. Myśliborski R, Latos-Grażyński L, Szterenberg L, Lis T. *Angew. Chem. Int. Ed*. 2006; **45**: 3670-3674.
3. Berlicka A, Latos-Grażyński L, Lis T. *Angew. Chem. Int. Ed*. 2005; **44**: 5288-5291.

4. Xue Z-L, Shen Z, Mack J, Kuzuhara D, Yamada H, Okujima T, Ono N, You X-Z, Kobayashi N. *J. Am. Chem. Soc.* 2008; **130**: 16478-16479.
5. Anju KS, Ramakrishnan S, Srinivasan A. *Org. Lett.* 2011; **13**: 2498-2501.
6. Pawlicki M, Garbicz M, Szterenberg L, Latos-Grażyński L. *Angew. Chem. Int. Ed.* 2015; **54**: 1906-1909.
7. Inokuma Y, Kwon JH, Ahn TK, Yoon MC, Kim D, Osuka A. *Angew. Chem. Int. Ed.* 2006; **45**: 961-964.
8. Makarova EA, Shimizu S, Matsuda A, Luk'yanets EA, Kobayashi N. *Chem. Commun.* 2008; 2109-2111.
9. Shiina Y, Karasaki H, Mori S, Kobayashi N, Furuta H, Shimizu S. *J. Porphyrins Phthalocyanines* 2016; **20**: 1049-1054.
10. Kobayashi N, Takeuchi Y, Matsuda A. *Angew. Chem. Int. Ed.* 2007; **46**: 758-760.
11. Takeuchi Y, Matsuda A, Kobayashi N. *J. Am. Chem. Soc.* 2007; **129**: 8271-8281.
12. Inokuma Y, Yoon ZS, Kim D, Osuka A. *J. Am. Chem. Soc.* 2007; **129**: 4747-4761.
13. Yoshida K, Copley G, Mori H, Osuka A. *Chem. –Eur. J.* 2014; **20**: 10065-10072.
14. Shimizu S, Matsuda A, Kobayashi N. *Inorg. Chem.* 2009; **48**: 7885-7890.
15. Inokuma Y, Osuka A. *Chem. Commun.* 2007: 2938-2940.
16. Shimizu D, Oh J, Furukawa K, Kim D, Osuka A. *Angew. Chem. Int. Ed.* 2015; **54**: 6613-6617.
17. Hirokawa S, Kobayashi N, Shimizu S. *Molecules* 2021; **26**: 1140.
18. Burla MC, Caliandro R, Camalli M, Carrozzini B, Cascarano GL, Giacovazzo C, Mallamo M, Mazzone A, Polidori G, Spagna R. *J. Appl. Crystallogr.* 2012; **45**: 357-361.
19. Sheldrick G. *Acta Crystallogr. Sect. A: Found. Crystallogr.* 2008; **64**: 112-122.
20. Frisch MJ, Trucks GW, Schlegel HB, Scuseria GE, Robb MA, Cheeseman JR, Scalmani G, Barone V, Petersson GA, Nakatsuji H, Li X, Caricato M, Marenich AV, Bloino J, Janesko BG, Gomperts R, Mennucci B, Hratchian HP, Ortiz JV, Izmaylov AF, Sonnenberg JL, Williams, Ding F, Lipparini F, Egidi F, Goings J, Peng B, Petrone A, Henderson T, Ranasinghe D, Zakrzewski VG, Gao J, Rega N, Zheng G, Liang W, Hada M, Ehara M, Toyota K, Fukuda R, Hasegawa J, Ishida M, Nakajima T, Honda Y, Kitao O, Nakai H, Vreven T, Throssell K, Montgomery Jr. JA, Peralta JE, Ogliaro F, Bearpark MJ, Heyd JJ, Brothers EN, Kudin KN, Staroverov VN, Keith TA, Kobayashi R, Normand J, Raghavachari K, Rendell AP, Burant JC, Iyengar SS, Tomasi J, Cossi M, Millam JM, Klene M, Adamo C, Cammi R, Ochterski JW, Martin RL, Morokuma K, Farkas O, Foresman JB, Fox DJ: Wallingford, CT, 2016.
21. Yanai T, Tew DP, Handy NC. *Chem. Phys. Lett.* 2004; **393**: 51-57.
22. Ditchfield R, Hehre WJ, Pople JA. *J. Chem. Phys.* 1971; **54**: 724-728.
23. Lu T, Chen F. *J. Comput. Chem.* 2012; **33**: 580-592.
24. Liu Z, Lu T, Chen Q. *Carbon* 2020; **165**: 461-467.
25. Crystallographic data for **2**. $C_{80}H_{56}B_2N_6O_2$, *Mw* = 1154.98, triclinic, space group *P*-1 (No. 2), a = 12.7019(11), b = 12.9170(12), c = 20.934(2) Å, α = 73.010(5), β = 83.864(6), γ = 64.880(5)°, V = 2973.4(5) Å^3, Z = 2, T = –173 °C, 55653 measured reflections, 10749 unique reflections (R_{int} = 0.1659), R = 0.0776 ($I > 2\sigma(I)$), R_w = 0.1968 (all data), goodness-of-fit on F_2 = 1.025, largest diff. peak/hole 0.30 and –0.25 e Å^{-3}.
26. Mack J, Stillman MJ, Kobayashi N. *Coord. Chem. Rev.* 2007; **251**: 429-453.
27. Kobayashi N, Muranaka A, Mack J. *Circular Dichroism and Magnetic Circular Dichroism Spectroscopy for Organic Chemists*; Royal Society of Chemistry: UK, 2012
28. Michl J. *J. Am. Chem. Soc.* 1978; **100**: 6801-6811.
29. Michl J. *Pure Appl. Chem.* 1980; **52**: 1549-1563.
30. Michl J. *Tetrahedron* 1984; **40**: 3845-3934.

31. Vancoillie S, Hendrickx M, Nguyen MT, Pierloot K, Ceulemans A, Mack J, Kobayashi N. *J. Phys. Chem. A* 2012; **116**: 3960-3967.
32. Gouterman M. *J. Chem. Phys*. 1959; **30**: 1139-1161.
33. Gouterman M. *J. Mol. Spectrosc*. 1961; **6**: 138-163.

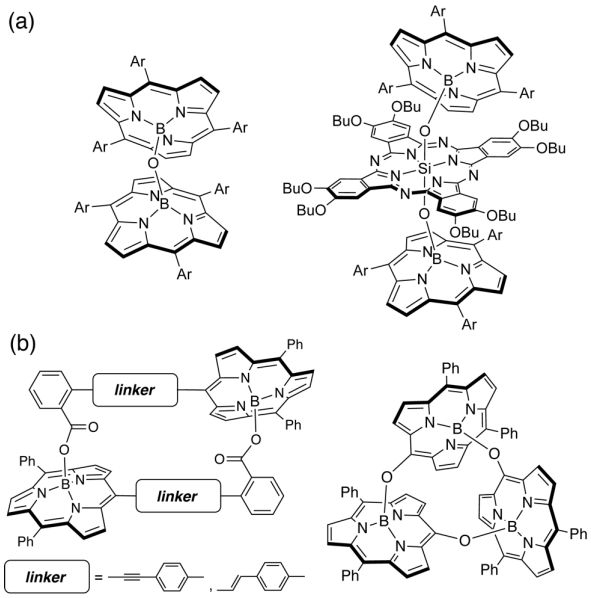

Fig. 1. (a) Face-to-face homo-dimer (left) and hetero-triad with phthalocyanine (right) and (b) head-to-tail homo-dimer (left) and homo-trimer (right).

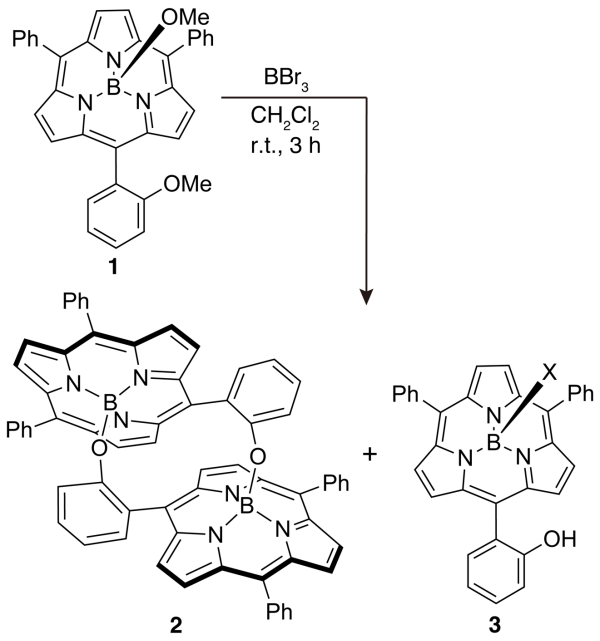

Scheme 1. Synthesis of the phenolate-bridged dimer (**2**) and *ortho*-hydroxyphenyl-substituted subporphyrin **3**. The axial ligand of **3** denoted by X was not determined.

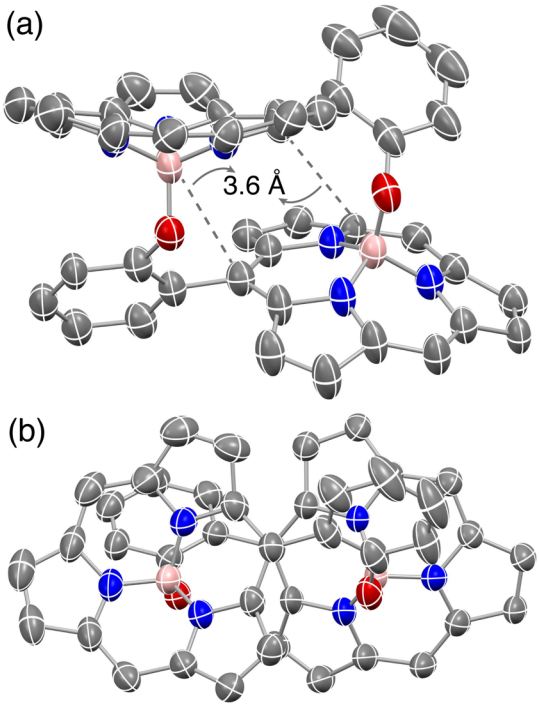

Fig. 2. X-ray single crystal structure of **2**, (a) side view and (b) top view. The thermal ellipsoids are scaled to the 50% probability level. Hydrogen atoms and *meso*-phenyl-substituents are omitted for clarity.

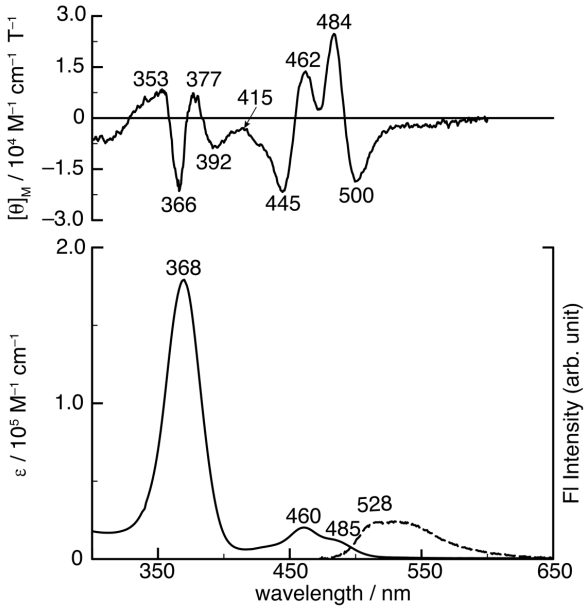

Fig. 3. UV/vis absorption (bottom, solid line), fluorescence (bottom, dashed line), and MCD (top) spectra of **2** in CH_2Cl_2.

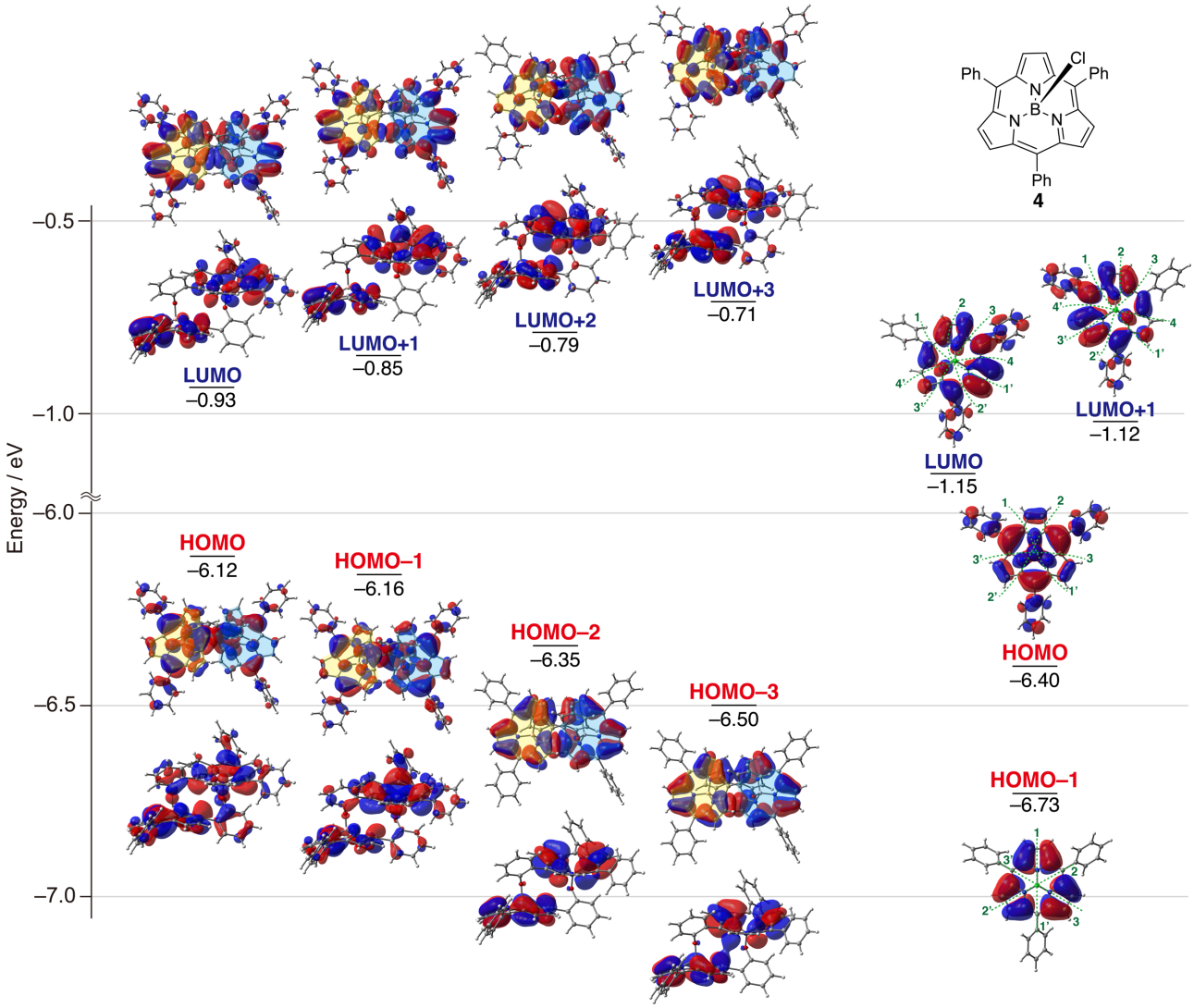

Fig. 4. Partial frontier MO diagram of **2** (left) and **4** (right) at the CAM-B3LYP/6-31G(d) level. Top (top) and side (bottom) views of MOs are shown for **2**. In the top views of **2**, subporphyrin cores are highlighted in light blue and yellow. Nodal planes of frontier MOs of **4** are shown by green dotted lines.